Monolayer Packing, Dehydration, and Ink-Binding Dynamics at the Molecular Printboard

ARTICLE *in* THE JOURNAL OF PHYSICAL CHEMISTRY C · APRIL 2009

Impact Factor: 4.77 · DOI: 10.1021/jp811189b

Monolayer Packing, Dehydration, and Ink-Binding Dynamics at the Molecular Printboard

Greg Gannon, J. Andreas Larsson, and Damien Thompson*

Tyndall National Institute, Prospect Row, Lee Maltings, Cork, Ireland

Received: December 18, 2008; Revised Manuscript Received: March 2, 2009

Gold-bound self-assembled monolayers (SAMs) terminating in β-cyclodextrin (β-CD) cavities provide a highly ordered surface array of hydrophobic binding pockets and so are used as "molecular printboards" for nanopatterning applications. The present work complements ongoing nanoscale experiments by providing the atom-scale structure, dynamics, and energetics of the printboard, which may aid the design of functional platforms for nanotechnology. We use fully atomistic molecular dynamics (MD) computer simulations to probe the printboard lattice constant, height, steric packing, hydrophobicity, and ink-binding properties as a function of gold−β-CD "linker" molecule and degree of binding to gold. The simulations reveal the stabilization associated with the experimentally observed surface lattice constant of ∼2 nm, alkanethioether linkers, and partial unbinding from gold. Additional ink-binding simulations indicate that multivalent ink molecules can offset disordering in the more loosely packed alkanethiol-linked printboard, with the attendant steric penalty similar in magnitude to the favorable multivalent ink:β-CD complexation.

Introduction

"Molecular printboards" exploit the self-assembly of alkanethiols on gold and the guest anchoring properties of β-cyclodextrin (β-CD) and have been used extensively for nanopatterning applications.[1,2] β-CD molecules can be tethered to surfaces such as gold and silicon oxide using long alkanethiol or alkanethioether "linker" chains, forming densely packed self-assembled monolayers (SAMs) on which uncharged "ink" molecules may be "printed" via hydrophobic guest:β-CD binding interactions. Molecules such as dendrimers[1,2] and macromolecules[3] including nanoparticles and biomolecules have been successfully immobilized on the printboard, providing highly ordered, functional arrays. Multivalent, or multisite, binding[12] enhances the overall complexation strength, providing a more robust but still electrochemically reversible patterning.[1,2]

Understanding the conformational properties and guest-binding abilities of functional aqueous/organic interfaces and membranes is central to the development of platforms for nanotechnology, of which the molecular printboard is a prime example, and also the development of biomedical technologies including targeted drug and gene delivery systems.[13−23] The structure and dynamics of β-CD molecules, dendrimers, and alkanethiol SAMs have been extensively probed using computational techniques (see, for example, refs 24−31 and references therein), and in the present work we use fully atomistic molecular dynamics (MD) simulations to probe the behavior of β-CD-terminated SAMs and describe their molecular structure, (de)hydration and multivalent-binding properties as a function of gold−β-CD linker molecule,[32] and degree of binding to gold.[33] We recently showed that the room-temperature binding of low-generation dendrimers can involve a payoff between favorable multisite complexation[34,35,24,25] and unfavorable steric strain,[26] the resulting partially bound orientations and "net energies" dictating both observed/nonobserved binding modes[35] and also the "effective concentration" of unbound ink anchor groups driving multivalent binding at the surface of the printboard.[34,1,2,27] Coarse graining the molecular models allowed us to access longer time scales and nonequilibrium behavior and illustrated a possible mechanism for molecular diffusion on the printboard via full dissociation and hopping between

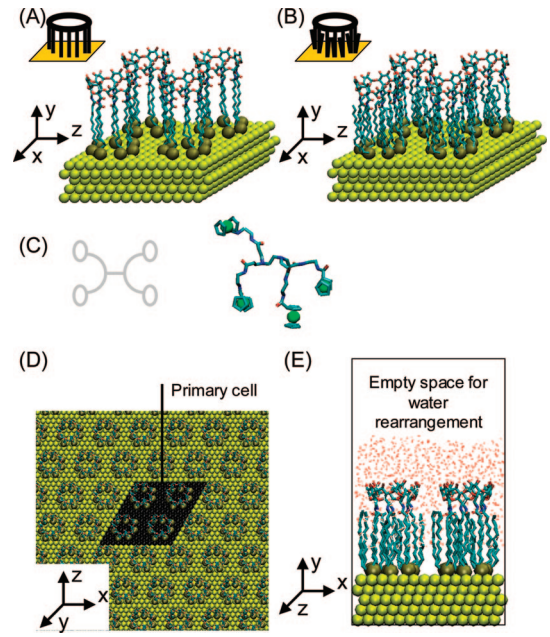

Figure 1. (A) Alkanethiol-linked and (B) alkanethioether-linked molecular printboard unit cells. Water molecules and all hydrogens are omitted for clarity. The gold (111) surface atoms are shown as yellow spheres, the sulfur atoms binding the molecules to gold are shown as tan spheres, and the terminal β-CD units and linker molecules are shown as sticks with carbons colored blue, oxygens red, and nitrogens blue. (C) G0-PAMAM-$(Fc)_4$ dendrimer molecule used in the ink-binding simulations. (D) Plan view of the hexagonally packed infinite printboard surface with lattice constant 2.06 nm, generated from the units cells shown in panels A and B: the primary cell is colored black. (E) Side view of a printboard unit cell illustrating the initial solvation conditions, including space for structural rearrangement of water molecules, as described in the text.

* To whom correspondence should be addressed. Phone: +353-21-490-4327. Fax: +353-21-427-0271. E-mail: damien.thompson@tyndall.ie.

10.1021/jp811189b CCC: $40.75
Published on Web 04/06/2009

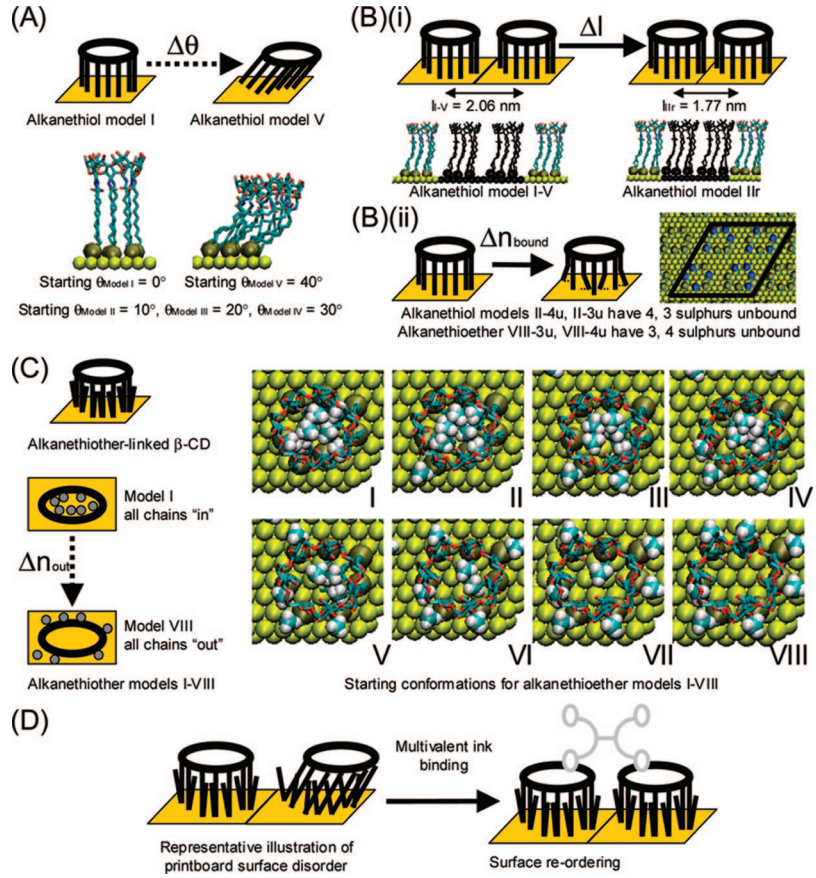

Figure 2. (A) How five different starting alkanethiol-linked printboard models I−V were generated by changing the initial linker tilt angle θ from 0° to 40° in increments of 10°. (B)(i) How alkanethiol-linked printboard model IIr (reduced) was generated, with the lattice constant l reduced from 2.06 to 1.77 nm; (B)(ii) how two alkanethiol-linked structures (IIr-4u and IIr-3u) and two alkanethioether-linked structures (VIII-3u and VIII-4u, see below) were built to model partially unbound Δn_{bound} printboard structures, in the representative example shown, by removing four out of seven sulfur−gold bonds (4u, 4 unbound in the nomenclature above) in each β-CD-linker unit, with unbinding sites determined using a random number generator and shown colored blue in the primary cell in the accompanying plan view of the printboard surface. (C) How eight different starting alkanethioether-linked printboard models I−VIII were generated by changing the initial orientation Δn_{out} of the alkane chain not directly bound to β-CD, from starting configuration I with $n = 0$, meaning all chains in the space directly underneath the β-CD units, to starting configuration VIII with $n = 7$, meaning all chains oriented "out", i.e., no chains in the space directly underneath the β-CD units. The resulting starting configurations I−VIII are shown in the accompanying plan view of the printboard surface, with the terminal CH_3 methyl groups on the alkanethioether alkane chain not directly bound to β-CD shown as spheres with CH_3 hydrogens shown explicitly and colored white. (D) How ink binding can "order" disordered regions of the printboard surface, as described in the text.

neighboring sites.[28] As well as applications in nanopatterning and more generally nanoelectronics, see, for example, "layer-by-layer" assembly,[36] multivalent binding at the molecular printboard may be exploited in the design of novel biosensors and therapeutic nanobiotechnology devices based on, for example, protein immobilization.[1−3,22,23]

In the present work, we use a series of multinanosecond MD simulations to describe the atom-scale dynamics and energetics of the molecular printboard in solution and when coated with multivalent molecules. These simulations allow us to describe the atom-scale interactions and resulting supramolecular structures giving rise to the experimentally observed[1,2] printboard lattice constant,[32] degree of attachment to gold,[33] and stabilization associated with alkanethioether linkers.[32] Furthermore, the role of dehydration and multivalent ink binding in surface function and ordering is described in terms of atom-scale dynamics.

Methods

Molecular models were constructed for the printboard as shown in Figure 1 with (a) alkanethiol and (b) alkanethioether chains linking the β-CD surface array to the gold (111) surface. A 3.4 × 3.0 × 4.0 nm box of water was overlaid, and waters overlapping the printboard were removed. To simulate coating of the surface with multivalent molecules, further models were generated with a divalently bound G0 ferrocene-terminated PAMAM dendrimer (Figure 1c) and a 3.4 × 5.0 × 4.0 nm water box overlaid to generate the solvated ink:printboard systems. Periodic boundary conditions were assumed; that is, the orthorhombic cell was replicated periodically in all directions, generating the infinite gold (111) surface and hexagonally packed printboard array shown in Figure 1d. Furthermore, the y axis was extended by 4.5 nm in each model, as shown in Figure 1e, to allow for net transport of water out of the printboard—the initial solvation strategy allowed for placement of water in between the linkers.

Standard CHARMM force field parameters[37] were used for β-CD and the PAMAM dendrimer, with the low-pH core and ferrocene anchors treated as described in refs 24−26. A slightly modified TIP3P model was used for the water.[38] Bonds involving hydrogen were constrained to their experimental lengths with the SHAKE algorithm,[39] allowing the use of a 2 fs time step for dynamics. We used the CHARMM program[40] version c31b2 for all calculations.

TABLE 1: Printboard Steric Energies and Structural Parameters[a]

linker group	starting configuration	steric energy E, kcal/mol	relative number of retained waters	lattice constant l, nm	height h, nm	tilt angle θ, deg
alkanethiol	I	−417(18)	8	2.1(0.2)	1.7 (0.1)	24(4)
alkanethiol	II	−445(14)	0	1.9 (0.3)	1.5 (0.1)	28(3)
alkanethiol	III	−443(15)	21	1.7 (0.3)	1.7 (0.1)	23(3)
alkanethiol	IV	−408(16)	34	2.2 (0.2)	1.5 (0.1)	38(8)
alkanethiol	V	−424(16)	38	2.2 (0.5)	1.6 (0.1)	37(6)
alkanethiol	IIr	−465(12)	3	1.7 (0.1)	1.7 (0.1)	18(2)
alkanethiol	IIr-4u	−494(11)	22	1.8 (0.1)	1.8 (0.1)	20(3)
alkanethiol	IIr-3u	−487(12)	17	1.6 (0.1)	1.7 (0.1)	23(3)
alkanethioether	I	−861(18)	23	2.0 (0.1)	1.8 (0.1)	9 (2)
alkanethioether	II	−844(17)	23	2.1 (0.1)	1.9 (0.1)	11(2)
alkanethioether	III	−853(14)	21	2.0 (0.1)	1.8 (0.1)	10(3)
alkanethioether	IV	−887(16)	9	1.9 (0.1)	1.8 (0.1)	13(4)
alkanethioether	V	−890(15)	17	2.0 (0.1)	1.7 (0.1)	13(4)
alkanethioether	VI	−881(16)	9	2.0 (0.1)	1.8 (0.1)	11(2)
alkanethioether	VII	−908(17)	3	1.9 (0.1)	1.7 (0.1)	10(2)
alkanethioether	VIII	−945(15)	2	2.1 (0.1)	1.7 (0.1)	13(2)
alkanethioether	VIII-3u	−933(15)	0	2.2 (0.4)	2.0 (0.1)	27(2)
alkanethioether	VIII-4u	−882(17)	7	2.0 (0.3)	1.9 (0.2)	31(6)

[a] Linker groups and starting configurations are as shown in Figures 1 and 2. Steric energy is calculated over all β-CD-linker printboard atoms, using 100 structures taken 1 ps apart along the final 0.1 ns of at least 2 ns of free dynamics. The relative number of retained water molecules is the minimum number of waters remaining within 0.5 nm of linker atoms, using 100 structures taken 1 ps apart along the final 0.1 ns of at least 2 ns of free dynamics, with values scaled so that the least hydrated alkanethiol and alkanethioether structures are set to zero. Lattice constant, height, and tilt angle were computed using the same structures as above. Standard deviations are in parentheses, averaged over both time and sites (for example, five structurally-nonequivalent β-CD−β-CD distances comprise the average lattice constant).

Two nanoseconds (2 ns) of molecular dynamics were performed (for each system) at constant, room temperature and pressure with a Nosé−Hoover algorithm, following 1.0 ns of thermalization and equilibration with gradually reduced positional constraints on the non-water molecules. Figure 2 shows the range of structures simulated. Solvated alkanethiol-linked printboard models were simulated initially in five different starting configurations corresponding to linker tilt angles θ of 0°, 10°, 20°, 30°, and 40° shown in Figure 2a(i). The lowest energy structure identified from multinanosecond molecular dynamics (see below) was then used to test the effects of lattice constant l (intermolecular spacing in the printboard units) and degree of sulfur−gold binding n_{bound} on printboard stability, as illustrated in panels i and ii of Figure 2b. Similarly, the solvated alkanethioether-linked printboard models (Figure 2c) were generated in eight alternative starting geometries, corresponding to different degrees of packing of the additional non-β-CD-bound alkane chain either underneath or between the β-CD units and the lowest energy MD structure (see below) used to test the energetics of partial unbinding from gold. Finally, two ink: printboard complexes were generated from representative equilibrated printboard configurations and used to test the effect of multivalent binding of printboard ordering, as illustrated in Figure 2d.

In all, over 50 ns of dynamics were performed and used to explore the conformational space of the bare and ink-bound printboard models, allowing us to identify the molecular structure of the printboard corresponding to the experimentally observed properties[1,2,32,33] and describe the effects of water and ink dynamics on printboard stability.

Results and Discussion

A. Fully Bound Alkanethiol-Linked Printboard Structures with Starting Lattice Constant 2.06 nm. Table 1 below quantifies the steric packing and structural properties of alkanethiol-linked printboard structures, generated from eight distinct starting structures featuring a range of different initial tilt angles (I−V), lattice constant (IIr), and degree of unbinding from gold (IIr-4u, IIr-3u), as described in the Methods above and illustrated in Figures 1 and 2. Focusing for the moment on alkanethiol-linked models I−V, fully bound with an initial 2.06 nm lattice constant, comparison of energetic/structural properties across models is instructive. The steric energies computed from structures following at least 2 ns of free dynamics indicate that structure II with an initial tilt angle of 10° generates the most stable structure (Table 1), which also features the strongest dehydration at near-linker regions, the second shortest lattice constant of 1.9 ± 0.3 nm, the joint lowest vertical height of 1.5 ± 0.1 nm, and moderate tilt angle of 28 ± 3°. Hydration data given in Table 1 was calculated from the number of water molecules retained in near-linker regions following at least 2 ns of free dynamics. Third-order polynomials drawn through both the steric energy and the hydration data in Figure 3A highlight the moderate correlation (0.6) between the two data sets; note this correlation drops to 0.3 upon inclusion of the two partially unbound models IIr-4u and IIr-3u. Correlation between data sets X and Y is expressed as the correlation coefficient $\rho_{(X,Y)} = \text{cov}(X,Y)/\sigma_X\sigma_Y$, where cov is the covariance and σ is the standard deviation, in this and all other reported correlation values. The lattice constant is the average distance between β-CD centers of mass, the height is the average distance between these centers of mass and the gold (111) surface, and the tilt angle is measured between the linker backbone and the plane normal to the gold surface Figures 3A and 4A illustrate how increasing dehydration, tighter packing, and the near-30° tilt angle typical of non-β-CD-capped alkanethiol SAMs[30] give generally more stable printboard structures.

B. Reduced Lattice Constant and Partially Unbound Alkanethiol-Linked Structures. Table 1 shows that Model IIr with a starting reduced lattice constant of 1.77 nm, as illustrated in Figure 2B(i), is significantly more stable than model II, the lowest energy 2.06 nm structure, and the stabilization is increased further upon release of 4 and to a lesser extent 3 sulfur−gold bonds (Models IIr-4u and IIr-3u), in agreement with X-ray photoelectron spectroscopy (XPS) measurements.[32,33] Furthermore, the general trend of increasing stability for shorter

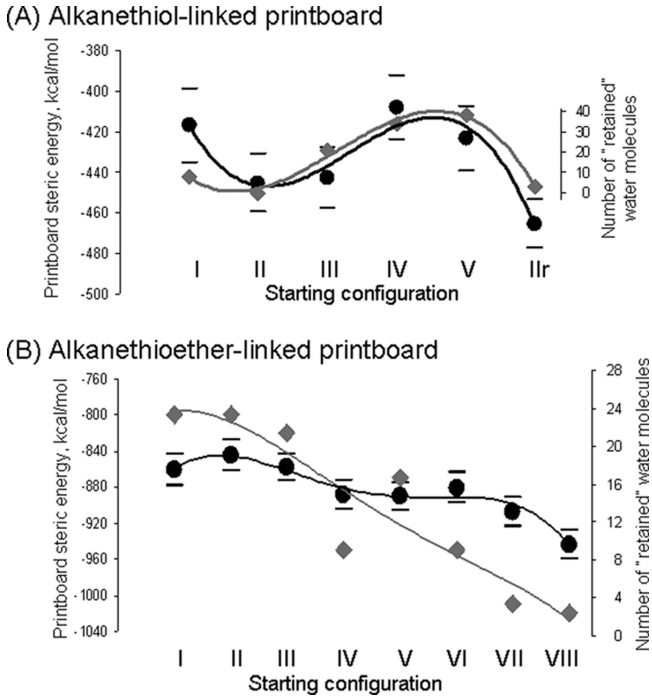

Figure 3. (A) Black data points plotted using the vertical axis on the left-hand side of the plot show time-averaged β-CD-alkanethiol molecule steric energies (kcal/mol) in the alkanethiol-linked molecular printboard, computed from 100 1 ps-spaced structures over the final 100 ps of dynamics. I−V and IIr on the horizontal axis label the six alternative starting configurations used. I−V are the five different tilt angle models shown in Figure 2A. IIr is the reduced lattice constant model shown in Figure 2B(i). Structures IIr-4u and IIr-3u, the two partially bound models based on model IIr with (IIr-4u) 4 and (IIr-3u) 3 of 7 sulfur−gold bonds released, as illustrated in Figure 2B(ii), are not included. Error bars show time-averaged standard deviations. Also plotted using the vertical axis on the right-hand side are the gray data points corresponding to the minimum number of water molecules "retained" within 0.5 nm of alkanethiol linker atoms over the final 100 ps of dynamics, calculated from the hydration data in Table 1. All values were computed following at least 2 ns of dynamics. (B) Steric energy and dehydration data for the alkanethioether-linked printboard model.

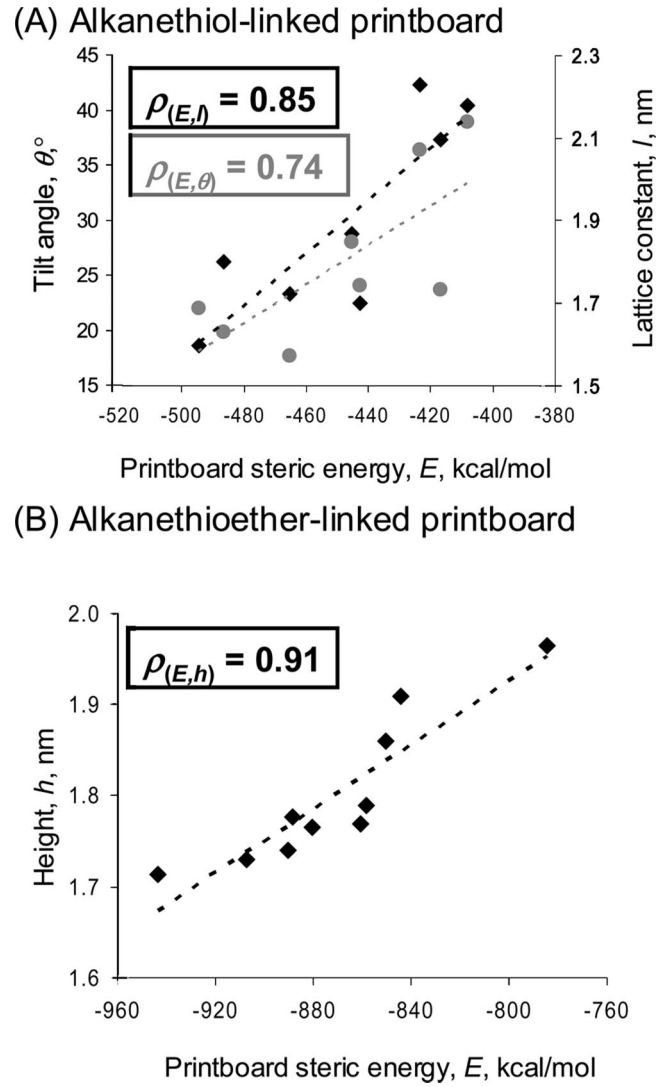

Figure 4. (A) Steric energy vs lattice constant and steric energy vs tilt angle for the alkanethiol-linked printboard, using all eight structures: I−V shown in Figure 2 together with structures IIr, IIr-4u, II-r3u, one reduced lattice constant model (IIr), and two partially bound models based on IIr with (IIr-4u) 4 and (IIr-3u) 3 of 7 sulfur−gold bonds released, as illustrated in Figure 2B(ii). Energy is plotted on the horizontal axis for convenience, with lattice constant and tilt angle on the two vertical axes. Correlation coefficients are also given and dotted best-fit lines drawn through the data sets to guide the eye. The principal "outlier" with respect to the best-fit line in the energy vs tilt angle data is the point at {−417, 24}, calculated from structures generated from starting model I with completely untilted alkanethiol chains (as shown in Figure 2A), arguably the most unrealistic of the starting alkanethiol models (see text). Error bars are not shown in the plots; they are given in Table 1. The correlation coefficient is <0.5 for steric energy vs height (not shown) in the alkanethiol-linked printboard. (B) Steric energy vs height for the alkanethioether-linked printboard, using all 10 structures: I−VIII shown in Figure 2 together with structures VIII-3u and VIII-4u, two partially bound models based on the low-energy alkanethioether model VIII with (VIII-3u) 3 and (VIII-4u) 4 of 7 sulfur−gold bonds released, as illustrated in Figure 2B(ii). The correlation coefficient is also given and a dotted best-fit line drawn through the data to guide the eye. Error bars are not shown in the plots; they are given in Table 1. Correlation coefficients are <0.5 for steric energy vs lattice constant and steric energy vs tilt angle (not shown) in the alkanethioether-linked printboard.

lattice constant and tilt angle below ∼30° holds across all alkanethiol models considered in the present study (Figure 4). Panel C in Figure 5 shows a plan view of the most stable fully bound alkanethiol structure IIr with reduced lattice constant. The surface ordering is similar to that obtained for the most stable partially unbound structure IIr-4u, shown in panels D and G of Figure 5 in plan and side views. This lowest energy alkanethiol model IIr-4u is proposed as the atom-scale structure of the alkanethiol-linked printboard used experimentally.[33] This structure maintains a lattice constant of 1.8 ± 0.1 nm, a relatively low tilt angle of 20 ± 3°, and a relatively large vertical height of 1.8 ± 0.1 nm. The partial unbinding of sulfur from gold thus allows for a slight increase in printboard height, though the expected attendant reduction in vertical steric packing is more than compensated for by the partial "filling" of intermolecular space by the less-constrained linker groups, illustrated in Figure 5G. The net energetic favorability of the partially unbound SAM compared to the fully bound SAM indicates that the experimentally observed partially bound structures[32,33] represent a thermodynamic minimum as well as a kinetically stable arrangement.

C. Bare and Ink-Bound Alkanethiol-Linked Printboard Structures. Shown in panels A−D of Figure 5 is a comparison between bare and ink-bound alkanethiol-linked structures, focusing on the inherently more disordered starting 2.06 nm lattice constant structures: the most stable structure II, and the most disordered structure V with the largest average lattice constant and also the largest time/site-averaged standard devia-

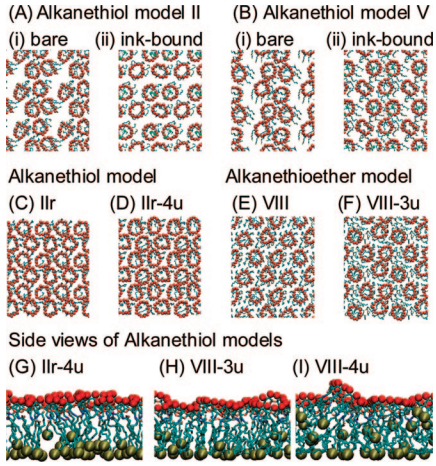

Figure 5. (A and B) Final structures for bare and ink-bound printboard models, following at least 2 ns of free dynamics, illustrating ink-induced printboard surface ordering. Data shown for two different alkanethiol-linked printboard models (A) II and (B) V. These models examine ink binding to (A) the most stable of the alkanethiol models with starting lattice constant 2.06 nm; (B) the most disordered of the alkanethiol models with starting lattice constant 2.1 nm (Table 1). Underlying gold atoms, waters and hydrogens are omitted for clarity. Printboard atoms are shown as sticks with oxygens on the primary rim of β-CD shown as red spheres to illustrate surface structure. Ink molecules are shown as lines in (A)(ii) and (B)(ii), with ferrocene central iron atoms shown as green spheres. Also shown for comparison are final structures obtained for bare printboard surfaces in panels C−F: (C) the alkanethiol model with reduced starting lattice constant 1.77 nm, IIr; (D) the proposed experimental alkanethiol model with shorter starting lattice constant 1.77 nm and 4 unbound sulfurs, IIr-4u; (E) the most stable of the (fully bound) alkanethioether models, VIII; (F) the alkanethioether model with 3 unbound sulfurs, VIII-3u. (G and H) Positions of unbound sulfurs in printboard structures IIr-4u and VIII-3u above, with surface β-CD oxygens shown as red spheres and linker sulfurs shown as tan spheres. (I) Positions of unbound sulfurs in the less stable alkanethioether structure VIII-4u with four unbound sulfurs.

tion in the individual β-CD−β-CD distances (Table 1). The structures in Figure 5A−D, together with the structural and energetic data in Table 2, clearly show the additional ordering imposed by binding ink molecules to the printboard. Ink-bound surfaces are more regular, with generally lower spread in inter-β-CD distances and also lower time-averaged deviations in the individual distances. Interestingly, the surface coverage of 1/2, attained via divalent binding to 2 of every 4 β-CD sites, appears to be sufficient to maintain more ordered surfaces, at least within the limits of the 4 β-CD unit cell and few nanosecond sampling times used.

In both cases also, ink-binding imposes a steric penalty on the SAM, the short-range nature of the linker−linker steric interactions means the more disordered bare structure with some β-CD-linker molecules closely packed and others well separated (Figure 5), is marginally more favorable than the structure with all β-CD-linker molecules at intermediate separations (Figure 5 and Table 2). Table 2 shows that the steric penalty incurred due to this decrease in SAM steric packing, is similar in magnitude to the favorable complexation energy due to the divalent binding,[34,35,24−26] suggesting that ink-binding can impose order on quasi-disordered printboard structures, with the favorable ink:printboard multivalent binding energy offsetting the steric SAM penalty. Higher order multivalent binding and also higher surface ink coverages may both be expected to increase this effect, given the additive nature of multivalent binding enthalpies[35,26] and the already well-ordered structures obtained with just 1/2 surface coverage; experimental testing of this hypothesis would be very interesting but is outside the scope of the present work.

TABLE 2: Comparison of (A) Printboard Lattice Constants and (B) Steric Energies for Bare Printboard Surfaces and Surfaces Complexed with Divalently-Bound G0-PAMAM(Fc)$_4$ Ink Molecules[a]

	II(bare)	II(inkbound)	V(bare)	V(inkbound)
(A) distance				
l_1	18.9 (1.1)	15.2 (1.1)	20.4 (1.0)	18.7 (1.0)
$\boldsymbol{l_2}$	14.9 (1.1)	**17.7 (0.6)**	26.2 (0.8)	**17.9 (0.8)**
l_3	19.0 (1.1)	18.1 (1.0)	17.6 (1.0)	21.1 (0.9)
l_4	24.2 (1.0)	22.3 (0.9)	17.8 (0.9)	21.2 (1.0)
l_5	16.5 (1.4)	17.7 (0.7)	29.5 (1.5)	19.8 (0.8)
(B) monolayer steric energies E (kcal/mol) and ink-binding induced monolayer steric penalty ΔE				
E	−445 (14)	−433 (14)	−424 (16)	−414 (11)
$\boldsymbol{\Delta E}$		**+12**		**+10**

[a] (A) Individual β-CD−β-CD separations comprising the average lattice constant l in bare surfaces and surfaces with one divalently bond G0-PAMAM-(Fc)$_4$ molecule per four surface β-CD sites, corresponding to an ink surface occupancy of one-half, together with (B) monolayer steric energies E (kcal/mol) in bare and ink-bound surfaces. Printboard models used are alkanethiol-linked structures II and V shown in Figures 2 and 5. (A) In each case l_2 is the β-CD−β-CD separation for the printboard binding sites complexing the divalently bound G0-PAMAM(Fc)$_4$ ink molecule, shown in bold. Ink-bound surfaces are more ordered, with generally lower spread in inter-β-CD distances and also lower time-averaged deviations in the individual distances. (B) Monolayer steric energy E calculated over all printboard atoms (not including waters, ink molecules, or gold surface atoms) using 100 structures taken 1 ps apart along the final 0.1 ns of at least 2 ns of free dynamics, with time-averaged standard deviations in parentheses. These E values in the ink-bound structures are compared with bare printboard energies (Table 1) to estimate ΔE, the steric penalty for ink-binding and "ordering" the printboard, preventing large shifts in inter-β-CD separations. In both cases, ΔE, shown in bold, is similar in magnitude to twice the binding enthalpy of approximately −6 kcal/mol per ferrocene:β-CD complexation (see text).

D. Atom-Scale Properties of the Experimental Alkanethioether-Linked Printboard Structure. From the energetic/structural data in Table 1 it is clear that the alkanethioether-linked structure with an initial "all-in" linker configuration, model VIII as illustrated in Figure 2, is significantly more stable than structures I−VII generated from starting models with some or all of the thioether chains not directly bound to β-CD oriented into the space between β-CD-linker molecules. The final lowest energy MD structure, which features 3−4 "out"-oriented linkers in each of the β-CD-alkanethioether molecules, is shown in plan view in panel E of Figure 5. This final MD structure, with starting "all-in" linker configuration, is significantly more stable than any structures generated from initial 3 "out" and 4 "out" configurations (Table 1), illustrating the need to consider many different starting models and produce multinanosecond MD trajectories to identify the atom-scale features of the ∼10 nm scale structures observed in atomic force microscopy (AFM) experiments.[33]

The general decrease in steric energy with dehydration in these eight fully bound alkanethioether-linked structures is similar to that observed above for the alkanethiol-linked structures and is shown in panel B of Figure 3, with fourth-order polynomials drawn through both data sets to highlight the strong correlation (0.9) between the two data sets; note this correlation drops to 0.1 upon inclusion of the two partially unbound models VIII-3u and VIII-4u. Panel B of Figure 4 includes also the partially unbound structures VIII-3u and VIII-

4u and shows the stability associated with lower vertical height. Neither tilt angle nor lattice constant show a significant correlation with steric energy, presumably due to the inherent higher order in the more tightly packed alkanethioether-linked printboard, as reflected in the generally lower standard deviations in the structural parameters for alkanethioether vs alkanethiol structures in Table 1. We note also that the most stable model VIII is only one of two structures which has a steady-state lattice constant of 2.1 ± 0.1 nm, coincident with the experimental AFM measurement,[33] though the range is admittedly very narrow, $(1.9-2.1) \pm 0.1$ nm over all the fully bound structures.

Panels F and H of Figure 5 show the partially unbound (3 sulfur−gold bonds released, to match XPS measurements[32,33]) alkanethioether-linked structure. Table 1 shows how partial unbinding slightly increases SAM height, similarly to the alkanethiol-linked printboard above, and more importantly, also allows the linkers to adopt an average near-30° tilt angle.[30] Model VIII-3u with three unbound sulfurs has a steric energy of -933 ± 15 kcal/mol, within the range of the fully bound structure (-945 ± 15 kcal/mol, Table 1). However, releasing an additional sulfur, model VIII-4u, shown in panel I of Figure 5, is not favorable, giving a large spread in tilt angles due to linker disordering (Figure 5I and Table 1), with this decrease in steric packing reflected in the large increase in steric energy ($E_{\text{VIII-4u}} = -882 \pm 17$ kcal/mol, Table 1) for release of the fourth sulfur. The observed lower degree of unbinding for the alkanethioether compared with alkanethiol structures[33] may thus be explained by the unbinding-induced decreased SAM packing due to linker disorder in the inherently closer-packed alkanethioether printboard compared with the unbinding-induced *increased* SAM packing due to linker disorder in the inherently more loosely packed alkanethiol printboard.

Conclusions

The present computational study has identified the molecular structures yielding the observed lattice constant and increased stabilization associated with alkanethioether linkers and partial unbinding from gold. Maximized steric packing in the SAM is achieved through reduced horizontal β-CD−β-CD surface separations (lattice constant), reduced vertical β-CD−gold distances (height), dehydration, tilt angles similar to non-β-CD-capped alkanethiol SAMs, and partial unbinding from gold. The difference in inherent packing between the alkanethiol and alkanethioether structures is illustrated through the reduced lattice constant calculated for the alkanethiol-linked printboard and also in the preferred extent of sulfur−gold unbinding, lower for the alkanethioether-linked printboard, in agreement with experiment.[32,33] Finally, binding multivalent inks to the printboard helps prevent large shifts in β-CD−β-CD separations in the more loosely packed alkanethiol-linked printboard, with the favorable multivalent ink:β-CD complexation compensating for the resultant steric penalty in SAM packing.

The detailed atom-scale structure, dynamics, and energetics of the molecular printboard, obtained from computer simulations on starting models incorporating known properties including lattice constants and degrees of binding, will aid the development of novel platforms for nanotechnology. Such aqueous/organic interfaces are the gate keepers that regulate the molecular interactions fueling living systems and are now also becoming ubiquitous in nanotechnology and bionanotechnology where binding at interfaces, and in some cases transport through interfaces, allows for the self-assembly of highly ordered functional "nanomachines" which may or may not incorporate some biocomponents. In this context, molecular printboards have proven to be robust, versatile, and selective platforms for nanotechnology, with multivalent molecular inks providing a means of anchoring nanoparticles and proteins to the functionalized SAM surface. Experimental testing remains the primary way of measuring key properties and behavior but cannot test everything; understanding the mechanisms requires detailed nanoscale experiments and simulations and so the present work focused on complementing experimental knowledge using atom-scale computer simulations.

Acknowledgment. This work was funded by the EC NaPa project (contract no. NMP4-CT-2003-500120). The authors acknowledge stimulating discussions with Jurriaan Huskens and Jim Greer. Calculations were performed at Tyndall National Institute using computer resources provided by Science Foundation Ireland (SFI) and also at the SFI/HEA Irish Centre for High-End Computing (ICHEC).

References and Notes

(1) Huskens, J. *Curr. Opin. Chem. Biol.* **2006**, *10*, 537–543.
(2) Ludden, M. J. W.; Reinhoudt, D. N.; Huskens, J. *Chem. Soc. Rev.* **2006**, *35*, 1122–1134.
(3) Ling, X. Y.; Reinhoudt, D. N.; Huskens, J. *Chem. Mater.* **2008**, *20*, 3574–3578.
(4) Ling, X. Y.; Phang, I. Y.; Reinhoudt, D. N.; Vancso, G. J.; Huskens, J. *Int. J. Mol. Sci.* **2008**, *9*, 486–497.
(5) Maury, P. A.; Reinhoudt, D. N.; Huskens, J. *Curr. Opin. Colloid Interface Sci.* **2008**, *13*, 74–80.
(6) Escalante, M.; Zhao, Y.; Ludden, M. J. W.; Vermeij, R.; Olsen, J. D.; Berenschot, E.; Hunter, C. N.; Huskens, J.; Subramaniam, V.; Otto, C. *J. Am. Chem. Soc.* **2008**, *130*, 8892–8893.
(7) Ludden, M. J. W.; Li, X.; Greve, J.; van Amerongen, A.; Escalante, M.; Subramaniam, V.; Reinhoudt, D. N.; Huskens, J. *J. Am. Chem. Soc.* **2008**, *130*, 6964–6973.
(8) Ludden, M. J. W.; Sinha, J. K.; Wittstock, G.; Reinhoudt, D. N.; Huskens, J. *Org. Biomol. Chem.* **2008**, *6*, 1553–1557.
(9) Ludden, M. L. W.; Mulder, A.; Schulze, K.; Subramaniam, V.; Tampe, R.; Huskens, J. *Chem.−Eur. J.* **2008**, *14*, 2044–2051.
(10) Escalante, M.; Maury, P.; Bruininkl, C. M.; van der Werf, K.; Olsen, J. D.; Timney, J. A.; Huskens, J.; Hunter, C. N.; Subramaniam, V.; Otto, C. *Nanotechnology* **2008**, *19*, 025101.
(11) Ludden, M. J. W.; Ling, X. Y.; Gang, T.; Bula, W. P.; Gardeniers, H. L. G. E.; Reinhoudt, D. N.; Huskens, J. *Chem.−Eur. J.* **2008**, *14*, 136–142.
(12) Choi, S.-K. *Synthetic Multivalent Molecules*; John Wiley & Sons, Inc.: New York, 2004.
(13) Kukowska-Latallo, J. F.; Bielinska, A. U.; Johnson, J.; Spindler, R.; Tomalia, D. A.; Baker, J. R. *Proc. Natl. Acad. Sci. U.S.A.* **1996**, *93*, 4897–4902.
(14) Eichman, J. D.; Bielinska, A. U.; Kukowska-Latallo, J. F.; Baker, R. J. *Pharm. Sci. Technol. Today* **2000**, *3*, 232–245.
(15) Gillies, E. R.; Frechet, J. M. *Drug Discov. Today* **2005**, *10*, 35–43.
(16) Lee, C. C.; MacKay, J. A.; Fréchet, J. M. J.; Szoka, F. C. *Nat. Biotechnol.* **2005**, *23*, 1517–1526.
(17) Wilson, S. P.; Yeomans, D. C.; Bender, M. A.; Lu, Y.; Goins, W. F.; Glorioso, J. C. *Proc. Natl. Acad. Sci. U.S.A.* **1999**, *96*, 3211–3216.
(18) Suh, J.; Wirtz, D.; Hanes, J. *Proc. Natl. Acad. Sci. U.S.A.* **2003**, *100*, 3878–3882.
(19) Batra, I. *Biomed. Microdev.* **2006**, *8*, 93. (b) Geng, Y.; Dalhaimer, P.; Cai, S. S.; Tsai, R.; Tewari, M.; Minko, T.; Discher, D. E. *Nat. Nanotechnol.* **2007**, *2*, 249–255.
(20) Lee, M.-T.; Hung, W.-C.; Chen, F.-Y.; Huang, H. W. *Proc. Natl. Acad. Sci. U.S.A.* **2008**, *105*, 5087–5092.
(21) Lundin, P.; Johansson, H.; Guterstam, P.; Holm, T.; Hansen, M.; Langel, U.; Andaloussi, S. E. L. *Bioconjugate Chem.* **2008**, *19*, 2535–2542.
(22) Villalonga, R.; Cao, R.; Fragoso, F. *Chem. Rev.* **2007**, *107*, 3088–3166.
(23) Ludden, M. J. W.; Huskens, J. *Biochem. Soc. Trans.* **2007**, *35*, 492–494.
(24) Thompson, D.; Larsson, J. A. *J. Phys. Chem. B* **2006**, *110*, 16640–16645.
(25) Thompson, D. *ChemPhysChem* **2007**, *8*, 1684–1693.
(26) Thompson, D. *Langmuir* **2007**, *23*, 8441–8451.
(27) Thompson, D. *J. Phys. Chem. B* **2008**, *112*, 4994–4999.
(28) Cieplak, M.; Thompson, D. *J. Chem. Phys.* **2008**, *128*, 234906.

(29) For a further recent example of dendrimer modelling, see, for example:Lin, S. T.; Maiti, P. K.; Goddard, W. A. *J. Phys. Chem. B* **2005**, *109*, 8663–8672.

(30) Gannon, G.; Larsson, J. A.; Greer, J. C.; Thompson, D. *Langmuir* **2009**, *25*, 242–247.

(31) Love, J. C.; Estroff, L. A.; Kriebel, J. K.; Nuzzo, R. G.; Whitesides, G. M. *Chem. Rev.* **2005**, *105*, 1103–1169.

(32) Beulen, M. W. J.; Bugler, J.; Lammerink, B.; Geurts, F. A. J.; Biemond, E. M. E. F.; Van Leerdam, K. G. C.; Van Veggel, F. C. J. M.; Engbersen, J. F. J.; Reinhoudt, D. N. *Langmuir* **1998**, *14*, 6424–6429.

(33) Beulen, M. W. J.; Bügler, J.; de Jong, M. R.; Lammerink, B.; Huskens, J.; Schönherr, H.; Vancso, G. J.; Boukamp, B. A.; Wieder, H.; Offenhäuser, A.; Knoll, W.; van Veggel, F. C. J. M.; Reinhoudt, D. N. *Chem.—Eur. J.* **2000**, *6*, 1176–1183.

(34) de Jong, M. R.; Huskens, J.; Reinhoudt, D. N. *Chem.—Eur. J.* **2001**, *7*, 4164–4170.

(35) Nijhuis, C. A.; Yu, F.; Knoll, W.; Huskens, J.; Reinhoudt, D. N. *Langmuir* **2005**, *21*, 7866–7876.

(36) Crespo-Biel, O.; Dordi, B.; Maury, P.; Péter, M.; Reinhoudt, D. N.; Huskens, J. *Chem. Mater.* **2006**, *18*, 2545–2551.

(37) MacKerrell, A. D.; Bashford, D.; Bellott, M.; Dunbrack, D. L.; Evanseck, J. D.; Field, M. J. *J. Phys. Chem. B* **1998**, *102*, 3586–3616.

(38) Jorgensen, W.; Chandrasekar, J.; Madura, J.; Impey, R.; Klein, M. *J. Chem. Phys.* **1983**, *79*, 926–935.

(39) Ryckaert, J. P.; Ciccotti, G.; Berendsen, H. J. C. *J. Comput. Phys.* **1977**, *23*, 327–341.

(40) Brooks, B. R.; Bruccoleri, R. E.; Olafson, B. D.; States, D. J.; Swaninathan, S.; Karplus, M. *J. Comput. Chem.* **1983**, *4*, 187–217.

JP811189B